A Numerical Investigation of Laminar flow over a Backward facing Inclined step

Aditya Mushyam[1]*, Josep M Bergada[1], C Navid Nayeri[2]

[1]Fluid Mechanics Department
Technical University of Catalunya
Terrassa, Barcelona, Spain-08222

[2] Hermann Föttinger Institute für Experimentelle Strömungsmechanik
Technical University of Berlin
Berlin, Germnay-10623

*Corresponding author

Corresponding Author:

Aditya Mushyam
Doctorate Researcher
Department of Fluid Mechanics
Technical University of Catalunya
Terrassa, Barcelona-08222

Email:mushyam.aditya@gmail.com
Phone:+34632771104
Fax: +34937398101

Second Author:
Josep M Bergada
Associate Professor
Department of Fluid Mechanics
Technical University of Catalunya
Terrassa, Barcelona-08222

Third Author:
C Navid Nayeri
Research Associate
Hermann Föttinger Institute für Experimentelle Strömungsmechanik
Technical University of Berlin
Berlin, Germnay-10623

A Numerical Investigation of Laminar flow over a Backward facing Inclined step

Aditya Mushyam[1]*, Josep M Bergada[1], C Navid Nayeri[2]

[1]Fluid Mechanics Department
Technical University of Catalunya
Terrassa, Barcelona, Spain-08222

[2] Hermann Föttinger Institute für Experimentelle Strömungsmechanik
Technical University of Berlin
Berlin, Germnay-10623

*Corresponding author

Abstract:
The aim of the present study is to analyze the two dimensional flow over a backward-facing-inclined step in laminar flow regime. The inspiration for the present work is derived from the fact that in automobile industry, analyzing the flow over an inclined step shall help in understanding the characteristics of the rear vehicle wake. A considerable percentage of the energy needed to propel the vehicle is dissipated by the vorticity generated in the rear of the vehicle, hence it is of utmost importance to understand the properties of the wake. In the present paper, the flow over a backward step is initially analyzed and the results are compared with the existing literature to validate the code developed. The inclined step simulations were carried out by varying different aspects of the geometry i.e. different tilts, several upstream lengths and a range of different Reynolds numbers. Critical Reynolds numbers for vortex shedding in the wake of different step inclinations have been analyzed for all cases studied. A discussion on the time-averaged drag and lift coefficients as a function of Reynolds number and for all cases undertaken, are among the results presented. Among the conclusions, it is particularly interesting to point out that the inclination angle of 15º was found to be the critical angle for vortex shedding, after which critical Reynolds number remains constant.

Keywords: Backward facing Step, Inclined Step, Critical Reynolds number, rolling up shear layer, Boundary layer, Laminar Flow

Nomenclature:

a	Height of the inclined step	(m)
C_D	Drag coefficient	
C_L	Lift coefficient	
F_D	Dimensional drag force	(N)
F_f	Flux through face f of the control volume	
F_L	Dimensional lift force	(N)
F_p	Dimensional normal force	(N)
F_s	Dimensional shear force	(N)
h	Height of the non-orthogonal physical domain	
l	Length of the non-orthogonal physical domain	
L_r	Non dimensional vortex recirculation length	
$\hat{n}$	Outward normal of the surface S	

p	Non dimensional Pressure	
Re	Reynolds number	
S	Surface onto the control volume	
t	Non-dimensional Time	
ul	Upstream Length of the physical domain	
u	Non-dimensional Velocity Y direction	
U	Free stream velocity in X direction at the inlet	(m/sec)
v	Non-dimensional Velocity Y direction	
$\forall$	Control Volume	(m^3)
x	Non-Dimensional Eulerian coordinates in horizontal direction	
x_p	Dimensional horizontal coordinate of the physical domain	(m)
y	Non-Dimensional Eulerian coordinates in vertical direction	
y_p	Dimensional vertical coordinate of the physical domain	(m)
δ	Non-Dimensional Boundary Layer thickness on the upstream surface	
η	Non-dimensional coordinates of transformed domain in vertical direction	
θ	Angle of inclination	(deg)
ξ	Non-dimensional coordinates of transformed domain in horizontal direction	

1. Introduction:

In the present study a two dimensional flow over a backward facing inclined step in laminar flow regime is analyzed. Most of the research undertaken until now has been focused on studying the flow over a backward-facing step. As a matter of fact, a comprehensive analysis of the flow over an inclined backward facing step has not been carried out. Flow past an inclined step is expected to have similarities to that of the backward facing case, hence this study was carried out to analyze the vortex dynamics associated with inclined step configurations. A brief introduction of some important research carried out on backward facing step and backward facing inclined step is presented in the following section. Some applications of the inclined step in the car industry shall also be discussed.

The interest in studying the flow over a backward facing step was intensified with the experimental and numerical work of Armaly et al (1983). They presented a detailed experimental investigation in a backward-facing step geometry located inside a rectangular channel for an expansion ratio H/h=1.94, where h and H are the inlet and outlet channel height respectively. An aspect ratio W/h=35 and Reynolds numbers ranging from 70 to 8000 were evaluated, W is the downstream channel length measured from the step. The flow appeared to be three-dimensional above Reynolds number 400. At this Reynolds number, a discrepancy between the experimental results and the numerical predictions was found regarding the primary recirculation length. A secondary recirculation zone was observed at the channel upper wall. This secondary recirculation zone was attributed for the discrepancy between experimental and numerical results. The normalized value of the reattachment length was maximum at Re 1200 and decreased for Reynolds numbers above 1200 due to the effect of Reynolds stresses.

Kim and Moin (1985) simulated the flow over a backward-facing step using a second-order accurate method in both space and time. They observed that dependence of the reattachment length on Reynolds number was in good agreement with the experimental data of Armaly et al (1983) up to Re=500, and started to deviate at Re=600. The difference was attributed to the three-dimensionality of the experimental flow around a Reynolds number of 600. Gartling (1990) developed a solution procedure using a Galerkin- based finite-element method for steady incompressible flow over a backward-facing step geometry. His results compared well with the results from Kim and Moin (1985) especially with respect to the bottom wall separation zone. Kaiktsis et al (1991) identified the bifurcation of two-

dimensional laminar flow to three-dimensional flow as the primary source of discrepancies appearing in comparisons of numerical predictions and experimental data. They also observed that irrespective of the accuracy of the numerical schemes, the experimentally measured recirculation lengths were consistently under-estimated above a Reynolds number of Re=600. It was reported that for Re>700 flow was unsteady and three-dimensional. In Kaiktsis et al. (1996), the flow was found to be convective unstable for Reynolds numbers ranging $700 \leq \mathrm{Re} \leq 2500$. A conclusion of this study was that the upstream-generated small disturbances propagated downstream at exponentially amplified amplitude with a space-dependent speed. Williams and Baker (1997) investigated the laminar flow over three dimensional backward-facing step geometry. They carried on a full three-dimensional simulation of the geometry used by Armaly et al (1983) for 100<Re<800 and found that the simulation correctly predicted the reattachment lengths and confirmed the effect of three-dimensionality. Armaly et al. (2003), reported the velocity measurements for three-dimensional laminar separated airflow adjacent to a backward-facing step using two-component laser Doppler velocimeter. They found that the flow was laminar and steady for Reynolds number smaller than 500. Some interesting flow features not visible in the two-dimensional studies were also observed in the experimental analysis presented in the paper.

Kaltenbach and Janke (2000) investigated the effect of sweep on the transitional separation bubble behind a backward-facing step using direct numerical simulation. The flow upstream of the step was laminar and shear-layer transition took place prior to reattachment. Further, Kaltenbach (2004) used Large Eddy Simulation to study turbulent flow over a swept backward facing step when Re_s = 5000 and for a range of swept angles. The configuration studied was the same as presented in Kaltenbach and Janke (2000). It was observed that the inclusion of a swept affected the dynamics of the near wall region upstream of the reattachment, upstream conditions strongly influenced flow dynamics, especially in the first half of the separation region.

Three dimensional laminar flow flowing inside a rectangular duct and over an inclined step was numerically studied in Chen et al (2006), the channel bottom wall was heated with constant head flux. Inclination slant angles of 0º, 45º, 60º and 75º were considered, angles were measured along a plane perpendicular to the flow field. Temperature, Nusselt number distributions, streamlines configuration and saddle and nodal points as a function of the inclination angle, were presented. The location where the streamwise velocity component was zero, at the center of the duct, changed from a saddle point to a nodal point as the inclination angle decreased. For small inclination angles, the maximum Nusselt number was located at the center of the duct. A single Reynolds number of 343 was used to perform the simulations. A set of different inclination angles 10, 15, 20, 25, 30 and 90 degrees, at Reynolds number 64000, has been recently studied in 2D and 3D using the Lattice-Boltzmann method in conjunction with large-eddy simulation, by Kotapati et al (2014). Among the results obtained, they presented the pressure and friction coefficients along the step surface, also the velocity profiles at several positions were obtained. Louda et al (2013) also performed a 2D and 3D numerical simulation over a facing step at different inclination angles, 10, 25, 45 and 90 degrees, Re_h = 15000, finite volumes and finite elements approaches were considered. As in Kotapati et al (2014), they presented as well the velocity distributions along the step surface, and compared their results with the experimental data obtained by Makiola (1992), in both cases, it was observed that the downstream vortex bubble length was independent of the step inclination angle.

Gandjalikhan Nassab et al (2009), studied the turbulent forced convection of flow progressing inside a rectangular duct where an inclined forward step was located. Flow was regarded as turbulent and they used the k-ε turbulence model to solve Navier-Stokes equations, non-orthogonal grid was transformed to orthogonal via using the Schwarz-Christoffel transformation. The channel bottom wall was heated at

a constant temperature. They concluded saying that the step length and inclination angle played a decisive role in the fluid hydrodynamic behavior. The near-wall flow over inclined and curved backward and forward facing steps was recently measured via using Particle image velocimetry (PIV) by Nguyen et al (2012). In this paper they presented an extension of the IPIV measuring technique previously developed by the authors. The new technique allows measuring tangential and wall normal velocity components and allows measuring the three velocity components when applied to stereoscopic PIV.

Cogotti (1998), studied experimentally the aerodynamic characteristics of a full scale simplified car model. Different parts of the car were modified to investigate the ground effect. This was the first time a systematic study into ground effect at full scale was published. In Leinhart et al (2003), flow measurements on an Ahmed body trailing edge were undertaken via using 2-component laser-Doppler anemometer. Two different slant angles of 25º and 35º were evaluated. Fluid used was air and the upstream incoming velocity was of 40 m/s. Kapadia et al (2003), numerically studied the flow on the trailing edge of an Ahmed car model with 25º slant angle. Spallart-Allamaras detached eddy simulation hybrid model and One-equation RANS model were used to perform the simulations. The paper also discussed the different turbulence modeling techniques available. Flow structure downstream was perfectly captured, static and dynamic drag coefficients were also analyzed. Krajnovic and Davidson (2004), modeled the flow over an Ahmed body with 25º slant angle via using LES, fluid was considered as incompressible, the flow Reynolds number based on the Ahmed body height was 7.68×10^5. Vortex generation on the car trailing edge was clearly seen. They realized that whenever the Reynolds number was high enough, a further increase of the Reynolds number had a small influence in the separated flow around a car. Guilmineau (2008), studied computationally the flow over an Ahmed body with two slant angles 25º and 35º. He used a flow solver called ISIS and unsteady Reynolds averaged Navier-Stokes equations URANS as turbulence model. Results were compared with other turbulence models. They had a good agreement for slant angle of 35º since the flow was mostly two dimensional, for 25º slant angle the flow was fully three-dimensional and they said further research was needed to properly model such flow. Franck et al (2009), applied Smagorinsky model modified with the Van Driest near wall damping, to study the flow over an Ahmed body with 12.5 degrees slant angle and was concluded that the model was feasible to study vehicle aerodynamics.

It can be said that a detailed analysis of inclination angle effects on flow past an inclined step, in laminar regime, has not been carried out with the different flow parameters deeply analyzed. This was a major inspiration for the present study along with the compelling similarity of the incline step geometry with the automobiles. Although the flow over automobiles is turbulent, the present study of the inclined step was carried out in laminar regime as a preliminary step towards understanding the effects of inclination the flow past the step.

2. Problem Statement:

Figure 1 presents the physical domain of the inclined step. In order to determine the effect of boundary layer on the downstream vorticity, several upstream lengths were evaluated. On the right hand side of the horizontal surface, it is found the inclined step. For the present paper, several inclination angles θ ranging from 5 to 75 degrees have been studied, also a comparison with previous studies undertaken by other researchers at $\theta=0$ degrees was carried out. Figure 1 also presents the dimensions of the inclined step and the boundary conditions used for the simulation. No slip boundary condition was used at all solid boundaries. As the flow is unconstrained at the top, a free slip boundary condition was used, and the open boundary was located at a distance of 8a, according to Sohankar et.al. (1995). Neumann boundary condition was used at the outlet. In order to simulate a far field downstream boundary, the

outlet boundary was located at a distance of 20a, downstream of the inclined step lower vertex, as suggested by Sohankar et.al. (1998).

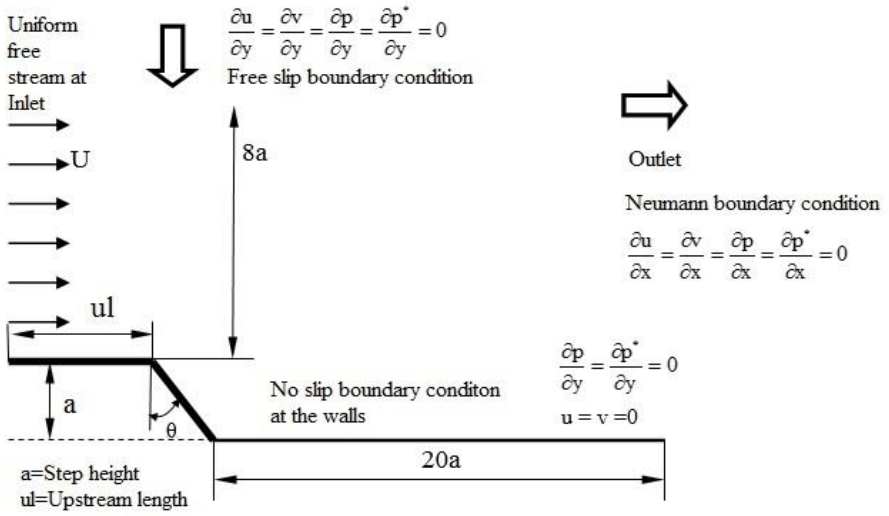

Figure 1: Physical Domain of the Inclined Step

Figures 2(a), (b), present the grid of the proposed problem. A non-orthogonal non uniform structured grid was chosen, since it is most appropriate to simulate the flow dynamics in the presence of an inclined edge. Figure 2b, shows the three sub domains used to generate the grid. The first sub domain is the region above the upstream horizontal surface, the second sub domain is the region starting at the vertex where the horizontal and inclined step meet, and covers the upper right hand side region. The grid region located on the right hand side of the inclined step wall is the third sub domain.

Structured grid has been generated in the three sub-domains using the stretching transformation proposed by Roberts (1971), which refines the grid in the vicinity of the solid walls. The domain on the right hand side of the inclined edge is transformed into an orthogonal domain by using a grid transformation as defined by Anderson (1995).

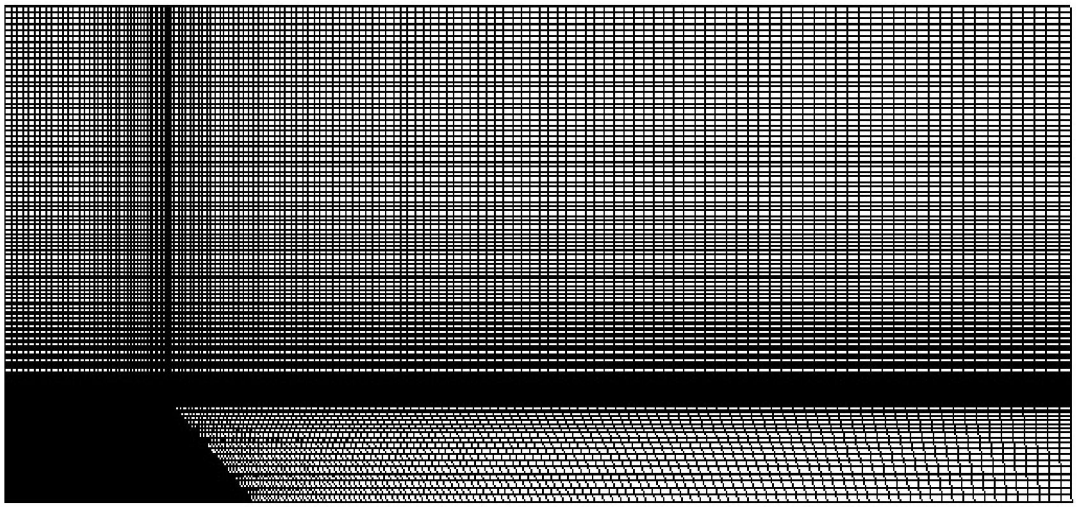

(a)

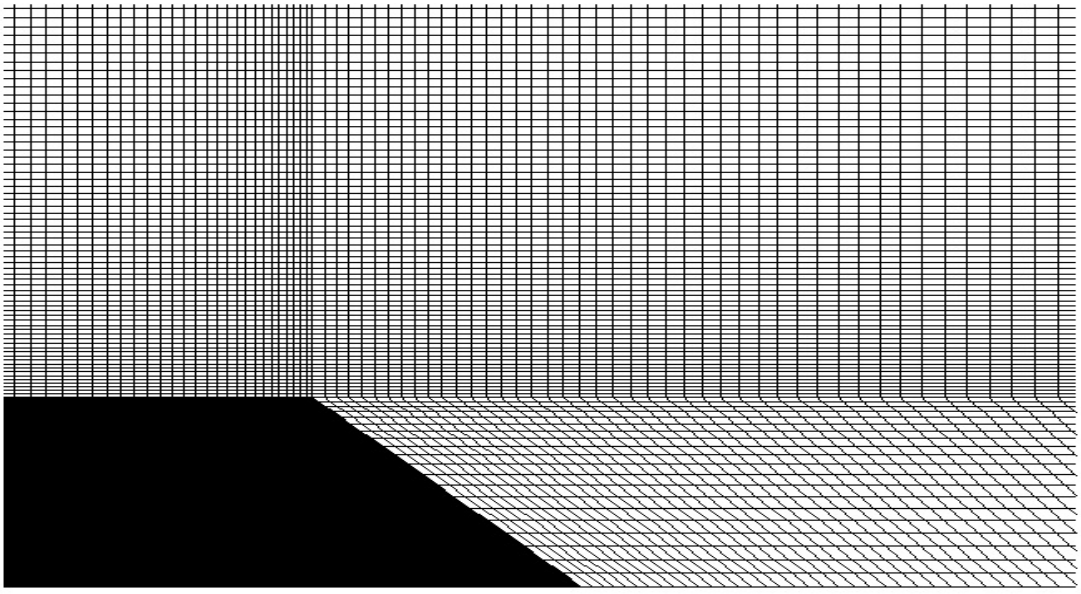

b)

Figure: 2(a) Non uniform structured grid for discretization of the domain. 2(b) Closer view of the grid point collocation at the wall of the step for accurate resolution of the boundary layer.

2.1 Governing Equations:

Simulations have been done with non-dimensional form of Navier-Stokes equations. To non dimensionalize the equations, the height of the step, a, was taken as the characteristic length, the free stream velocity U was taken as the characteristic velocity, the characteristic pressure was ρU^2, the characteristic time was defined as the characteristic length divided by the characteristic velocity a/U and the characteristic frequency was U/a. Reynolds number was defined as $\mathrm{Re} = \frac{\rho U a}{\mu}$; notice that fluid density and viscosity were taken as constant. Flow was considered as isothermal.

The non-dimensional form of the momentum and continuity equations for laminar flow is represented as:

$$\frac{\partial u}{\partial t} + \frac{\partial u\,u}{\partial x} + \frac{\partial vu}{\partial y} = -\frac{\partial p}{\partial x} + \frac{1}{\mathrm{Re}}\left(\frac{\partial^2 u}{\partial x^2} + \frac{\partial^2 u}{\partial y^2}\right) \tag{1}$$

$$\frac{\partial v}{\partial t} + \frac{\partial uv}{\partial x} + \frac{\partial vv}{\partial y} = -\frac{\partial p}{\partial y} + \frac{1}{\mathrm{Re}}\left(\frac{\partial^2 v}{\partial x^2} + \frac{\partial^2 v}{\partial y^2}\right) \tag{2}$$

$$\frac{\partial u}{\partial x} + \frac{\partial v}{\partial y} = 0 \tag{3}$$

The finite volume approach was chosen for the simulation

2.2 Numerical Strategy and Boundary Conditions:

A second-order Adams Bashforth-Crank Nicholson scheme for temporal discretization was applied to

Navier Stokes equations in finite volume formulation to obtain equation (4). Equation (5) is the continuity equation applied over a control volume.

$$\frac{u_{i,P}^{n+1}-u_{i,P}^{n}}{\Delta t}V_P+\left(\frac{3}{2}\sum_f F_f^n u_{i,f}^n-\frac{1}{2}\sum_f F_f^{n-1}u_{i,f}^{n-1}\right)=-\sum_f p_f^n S_{f,i}+\frac{1}{2\,\mathrm{Re}}\left(\sum_f F_{dfi}^{n+1}+\sum_f F_{dfi}^{n}\right) \quad (4)$$

$$\sum_f F_f^{n+1}=0 \quad (5)$$

Equations (4) and (5) were solved by using the bi-conjugate gradient stabilized method.
The boundary conditions used in the simulation were depicted in figure 1, a brief description of the different boundary conditions follows.

At the inlet, uniform free stream condition for velocity and Neumann boundary condition for pressure were used.

$$u=U,\quad v=0,\ \frac{\partial p}{\partial x}=0 \quad (6)$$

In all solid boundaries, no-slip boundary condition for velocity and normal gradient condition for pressure was employed.

$$u=0, v=0 \text{ and } \nabla p.\hat{n}=0 \quad (7)$$

Where $\hat{n}$ is the unit normal vector perpendicular to the surface.

At the far field, as the present study focuses on the unconfined flow past an inclined step, a free slip boundary was applied at a distance of 8a, measured from the upstream horizontal surface, see figure 1.

$$\frac{\partial \phi}{\partial y}=0;\ \phi=u,v;\ \frac{\partial p}{\partial y}=0 \quad (8)$$

The outlet boundary, right hand side of figure 1, posed the biggest difficulty in computational modeling, especially when studying flows with unsteady wake or convecting vortices. The definition of this boundary condition is of paramount importance, since it not only changes the flow pattern but also affects convergence. For the present case the derivative of all dependent variables was taken equal to zero, which is known as Neumann boundary condition (NBC), condition presented in equation (9).

$$\frac{\partial \phi}{\partial x}=0,\ \phi=u,v,p; \quad (9)$$

The distance between the inclined step bottom edge and outlet boundary, where the Newman boundary condition is applied, was considered as 20a as seen in figure 1.

MAC (Marker and Cell) method with velocity and pressure coupling was applied using a predictor-corrector strategy. In the present study, the respective pressure correction factor in all the neighboring cells were also considered, notice that this is a further improvement with respect to the original MAC

method and minimizes the error involved in the calculation. In this method the momentum equations are solved to calculate provisional values for the velocity components for the next time step using the predictor step and thereafter calculating the pressure and velocity correction factors for achieving the incompressibility condition of mass conservation.

For the inclined step case, the grid located on the right hand side of the inclined boundary edge, has a non-orthogonal domain, (x,y) this domain was transformed into an orthogonal domain (ξ, η).

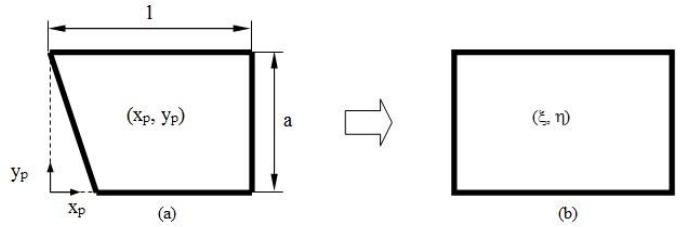

Figure: 3. Transformation of the physical domain to computational domain (a) Physical domain (b) Computational domain

The transformation equations used to transform the physical domain to a computational domain are presented as equations (10), (11) and (12).

$$\xi = \left(\frac{x_p - c}{l - c} \right) \tag{10}$$

$$\eta = \left(\frac{y_p}{a} \right) \tag{11}$$

Where l and a are the length and height of the physical domain as shown in figure 3 and c is a constant defined by:

$$c = \left(\frac{a - y_p}{\cot\theta} \right). \tag{12}$$

To transform Navier-Stokes equations from non-orthogonal to orthogonal coordinates, the transformation mentioned in Anderson (1995) was used, for the first and second derivatives.

The non-dimensional form of momentum and continuity equations, (1) to (3), can be transformed into equations in the orthogonal domain, equations (13) to (15) using transformation equations (10) to (12)

$$\frac{\partial u}{\partial t} + \xi_x \frac{\partial uu}{\partial x} + \eta_y \frac{\partial vu}{\partial y} = -\xi_x \frac{\partial p}{\partial x} + \frac{1}{Re}\left(\xi_x^2 \frac{\partial^2 u}{\partial x^2} + \eta_y^2 \frac{\partial^2 u}{\partial y^2} \right) \tag{13}$$

$$\frac{\partial v}{\partial t} + \xi_x \frac{\partial uv}{\partial x} + \eta_y \frac{\partial vv}{\partial y} = -\eta_y \frac{\partial p}{\partial y} + \frac{1}{Re}\left(\xi_x^2 \frac{\partial^2 v}{\partial x^2} + \eta_y^2 \frac{\partial^2 v}{\partial y^2} \right) \tag{14}$$

$$\xi_x \frac{\partial u}{\partial x} + \eta_y \frac{\partial v}{\partial y} = 0 \tag{15}$$

The transformed equations, (13) to (15), can be discretized using the second-order Adams Bashforth-Crank Nicholson scheme, as it was previously used to discretize the non-dimensional equations (1) to (3), into (4) and (5).

3. Code Validation:

The code was validated by simulating the flow over a backward step and the results were compared with the results presented in the literature. Figure 4 presents the streamline plots for the backward facing step case. The left hand side of the figure, presents the results obtained from the code developed and the graphs presented on the right hand side, were obtained by Chowdhary and Dhiman (2011). Three Reynolds numbers of 100, 150 and 200 were studied in both cases. The comparison was in complete agreement in all cases studied, flow configuration was very much alike, the downstream vortices were steady in all cases and their respective length was the same in all comparisons undertaken. It is necessary to point out that as the plots presented in the right hand side of figure 4 were extracted from Chowdhary and Dhiman (2011), their quality has been compromised when reducing their dimensions. A grid of size (200x150), with 50 and 40 cells on the upstream and inclined surface of the step respectively, was used to simulate the flow in these validation cases.

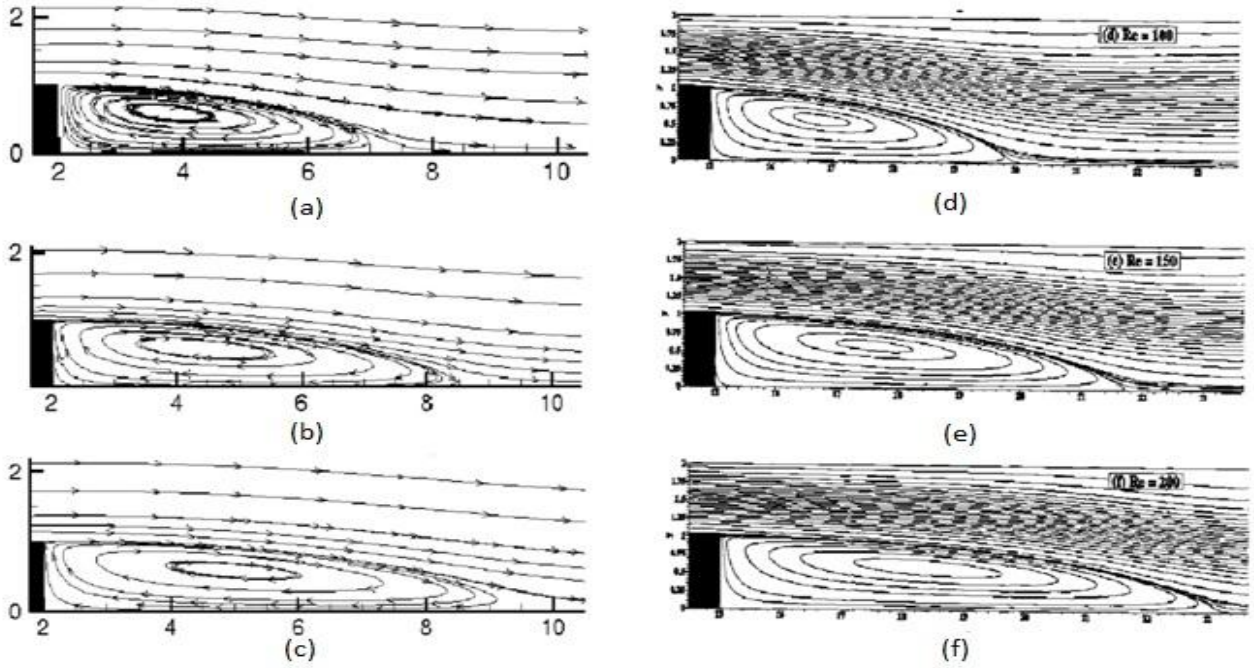

Figure 4: Instantaneous Streamline plots for Reynolds Numbers: (a), (d) Re=100, (b), (e) Re=150 and (c), (f) Re=200. Left hand side figures were generated by the present code, right hand side figures were created by Chowdhary and Dhiman (2011).

From the present code, it has also been found, from a further analysis of the backward step geometry and for a flow simulation at Reynolds 498, that downstream vortex flow was steady, on the other hand, when Reynolds number was 500, downstream flow became unsteady and periodic. It therefore can be inferred that the onset of vortex shedding is observed to be around Reynolds number 500, as found originally by Armaly et al (2003), also Chen et al (2006) mentioned this flow behavior. They pointed out that the critical Reynolds number, for flow transition from steady state to unsteady periodic vortex dissipation in the wake of the backward step, was around 500.

3.1 Effect of Grid Refinement:

A grid refinement study has been carried out on three progressively refined grids, namely 160×140, 200×150 and 220×160 where the number of grid nodes distributed over the inclined edge of the step are 30, 40 and 50, respectively. An inclination angle, $\theta=60^0$ and ul=4a was considered for the grid refinement study at Reynolds number, Re=500. During the refinement, the smallest and the largest cell size on the inclined edge is maintained approximately at 0.02 and 0.033, respectively.

Grid	160x140	200x150	220x160
Drag Coefficient, C_D	0.2092673	0.2110388	0.2116015
Strouhal Number, St	0.05	0.05	0.05

Table 1: Results of the grid refinement study

The variation in the drag coefficient, C_D was 0.85% when the grid was refined from coarsest to the intermediate level. But when the grid was further refined to the finest level, the variation reduced to 0.27%, see table 1. Therefore based on these results, a grid size of 200x150 was considered for the simulation with ul=2a and 4a and for ul=a, a grid size of 160x150 was used for all Reynolds numbers.

4. Results and Discussion:

In order to evaluate the flow over and inclined backwards facing step, the results for various simulations carried out will be presented in this section. Simulations were performed for an inclination angles of, θ = 15º, 30º, 45º, 60º and 75º, three different upstream lengths of ul=a, ul=2a and ul=4a were chosen, to study the boundary layer development on the horizontal surface and also to analyze the effects of boundary layer on the wake of the flow past an inclined step. Firstly the steady state flow will be presented for inclination angles, θ =15º, 30º, 45º, 60º and 75º, upstream channel lengths of ul=4a and Reynolds numbers of 100, 200, 349 and 350. Reynolds numbers 349 and 350 were analyzed to understand the flow transition from steady to unsteady. Simulations for angles of inclination, θ =5º, 10º, 12º, 14º were undertaken to analyze the trend followed in the angles less than θ =15º for attaining criticality. Secondly, the unsteady flow analysis for the same angles and upstream lengths ul=a, 2a and 4a are presented for Reynolds numbers Re = 500 and 800. The temporal averaged and dynamic lift and drag coefficients are also presented in the final part of this section.

4.1 Boundary Layer development on the upstream surface, ul:

The development of the boundary layer on the upstream surface length, ul plays an important role in the dynamics of the flow past an inclined step. Three different upstream lengths ul=a, 2a and 4a were simulated to understand evolution and development of the boundary layer and its effects on the flow properties.

For the inclined step geometry with ul=a and all inclination angles a grid of size (160x150) was used with 20 cells on the upstream surface. Similarly for the step with ul=2a and 4a and for all inclination angles, a grid size of (200x150) was used with respectively 40 and 50 cells on the upstream surface. In all cases, for different upstream lengths and inclination angles, 40 cells have been used on the inclined surface. The time step was considered as 0.001. The same grid size was used in both steady and unsteady flow cases. Figure 5 presents instantaneous vector plots over the upstream surface of the step for all different upstream lengths, ul. Figure 5(a) and (b) respectively present the boundary layer development for Re=500 and Re=800, for upstream length ul=4a. The boundary layer thickness, δ at the step corner is similar for both cases, with $\delta\approx0.2$ as presented in Figure 5(a) and (b). A similar thickness value of $\delta\approx0.2$ can be found for ul=2a in figure 5(c), but in figure 5(d) for ul=a, the boundary

layer thickness, δ reduces to approximately 0.15. This can be attributed to the shorter upstream length, ul=a, which is not sufficient for the complete development of the laminar boundary layer which appears to be fully developed for ul=2a and remains constant until ul=4a. It can be inferred that a minimum of ul=2a is needed for the laminar boundary to develop completely. This can also be seen as a validation for the grid used for simulating different upstream lengths. The width of the cell on the upstream surface is 0.032, the width of the boundary layer for ul=2a and 4a accommodates approximately 6 cells of the refined grid near the upstream surface. In the case of ul=a, about four cells are contained inside the boundary layer at the inclined step upper vertex.

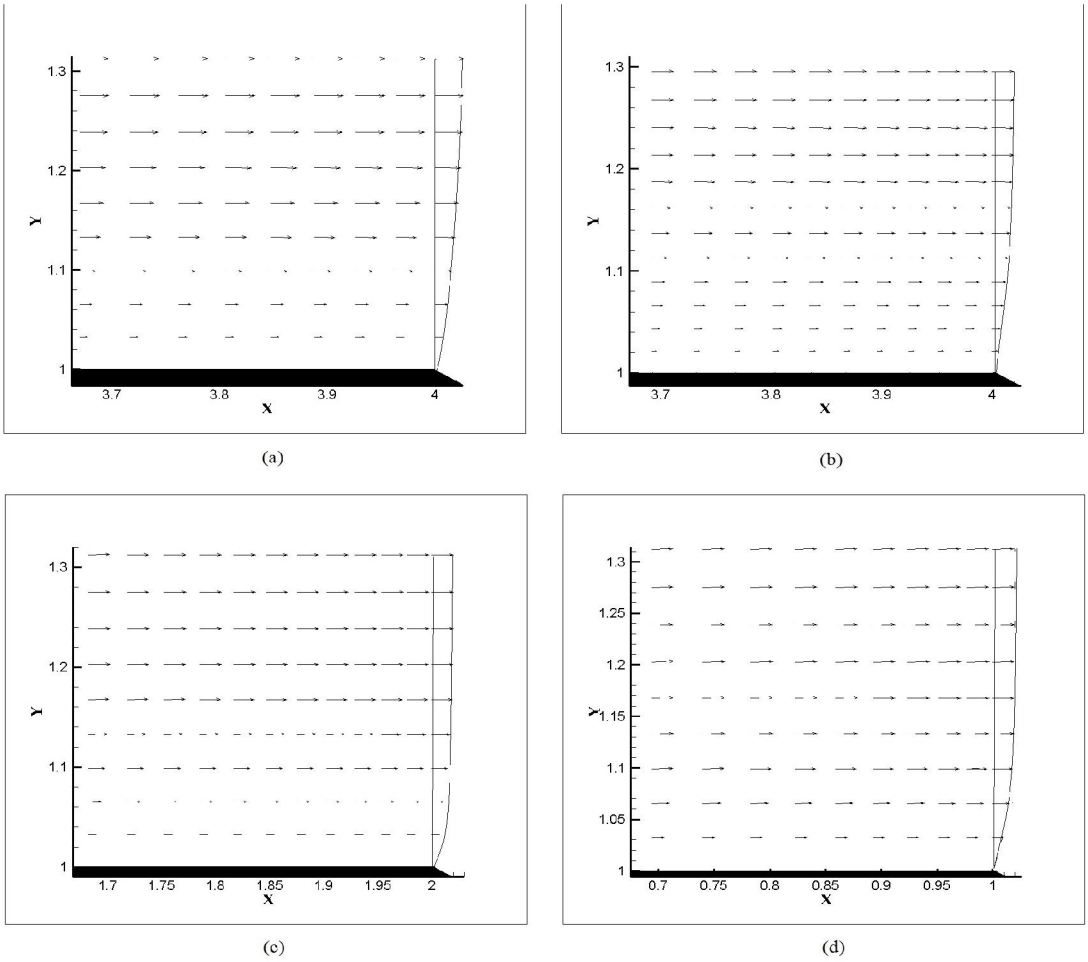

Figure 5: Instantaneous vector plots on the upstream surface, ul for θ=60º (a) Re=500, ul=4a, (b) Re=800, ul=4a, (c) Re=500, ul=2a and (d) Re=500, ul=a.

4.2 Steady state flow analysis:

Figures 6 and 7 show the steady state analysis. In each figure, five different inclination angles of θ =15º, 30º, 45º, 60º and 75º for a single Reynolds number and upstream length, ul=4a were studied. Figure 6 presents Reynolds number, Re=100 and 200 and figure 7 presents Re=349. When simulating flow at Reynolds number, Re=350 for all five inclination angles, downstream vortical flow was found to be unsteady, periodic vortex shedding appeared in all cases. During the simulations it was realized that the modification of the upstream length produced no appreciable variation in the flow properties, since the boundary layer development is similar for different lengths and not affecting much the flow past the inclined step.

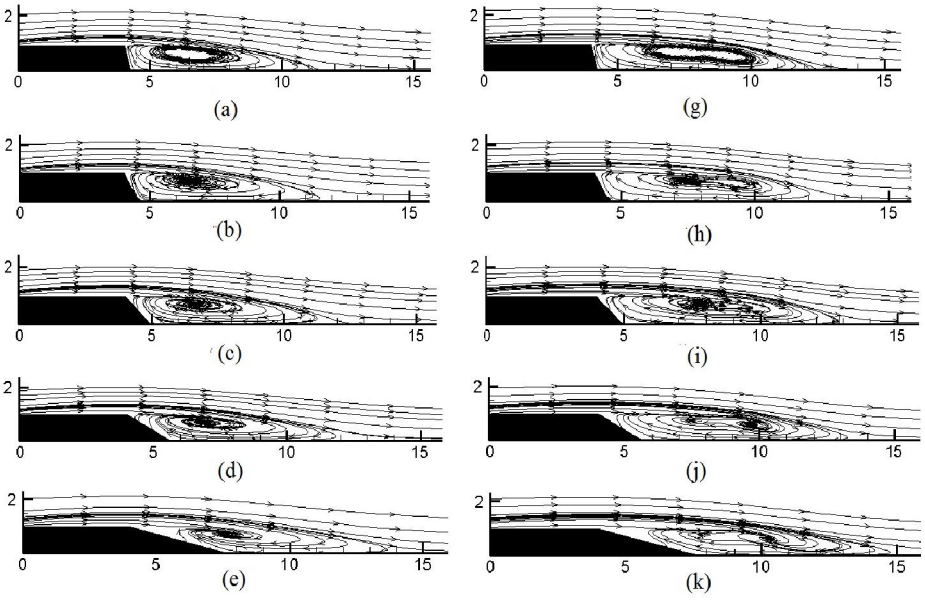

Figure 6: Steady state streamline plots for Reynolds Number 100 for inclination angles. a) θ=15º, b) θ=30º, c) θ=45º, d) θ=60º, (e) θ=75º and Reynolds number 200 for inclination angles. (g) θ=15º, (h) θ=30º, (i) θ=45º, (j) θ=60º, (k) θ=75º Upstream channel length ul=4a.

When comparing figures 6 and 7, it can be noticed that for a given Reynolds number, the downstream static recirculation vortex length, remains pretty much constant and independent of the inclination angle. Similar phenomenon was also reported by Chen et.al. (2006), Kotapati et.al. (2014) and Makiola et.al. (1992). Downstream static recirculating vortex length (L_r) increases with the increase of Reynolds number. The variations of recirculating vortex length (L_r) were calculated for three different static cases, Reynolds numbers Re=100, 200 and 349, their respective values were fitted into a polynomial to obtain a relation given in equation (16).

$$L_r = (-4.96804\text{x}10^{-12})Re^5 + (3.31561\text{x}10^{-9})Re^4 - (2.11322\text{x}10^{-7})Re^3 - (2.77175\text{x}10^{-4})Re^2 + (7.72119\text{x}10^{-2})Re + 9.75374\text{x}10^{-6} \quad (16)$$

4.3 Critical Reynolds number for onset of vortex shedding:

The point of criticality at which flow becomes unsteady and periodic from steady state is called the critical Reynolds number. $Re=Re_{cr.}$

From figure 7 it can be seen that the flow is steady for all angles from 15º to 75º until Reynolds number 349. The critical Reynolds number for angles of inclination from 15º to 75º was found to be 350, since the flow was unsteady and periodic at Re=350. It was also determined that for angles below θ=15º flow behavior was different with respect to the criticality, it appears as if critical Reynolds number decreases as the angle of inclination is increased from θ=0º to θ=15º. To analyze this trend of the flow characteristics for angles of inclination smaller than 15º, at small Reynolds numbers, a set of new simulations were carried out for θ=5º, 10º, 12º, and 14º, at Reynolds numbers, Re=350, 351, 352, 358, 359, 360, 370, 372, 375, 380, 382, 385, 400, 404 and 405 in order to determine their respective critical Reynolds numbers. Therefore a critical angle of inclination is expected, all angles of inclination above which will have the constant critical Reynolds number for the flow to become periodic and unsteady.

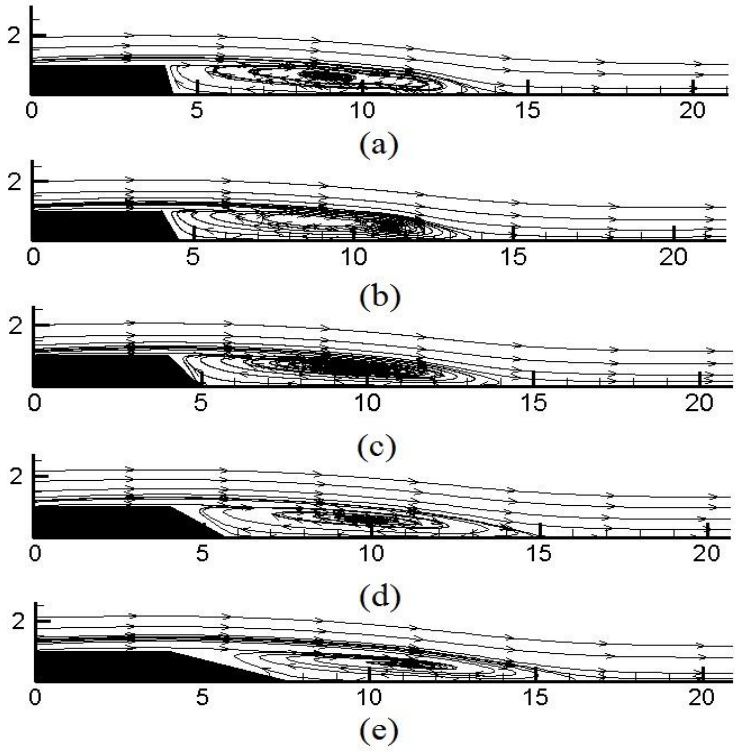

Figure 7: Steady state streamline plots for Reynolds Number 349 and inclination angles. (a) θ=15º, (b) θ=30º, (c) θ=45º, (d) θ=60º and (e) θ=75º Upstream channel length ul=4a.

It was determined from the simulations that flow is steady when θ=5º, 10º, 12º and 14º at Reynolds number, Re=404, 374, 359 and 351 respectively, which implies that the critical Reynolds number for these angles of inclination is above 350. Therefore it can be concluded that the critical angle of inclination is θ_{cr}=15º, above which the flow critical Reynolds number, Re_{cr}=350, remains constant.

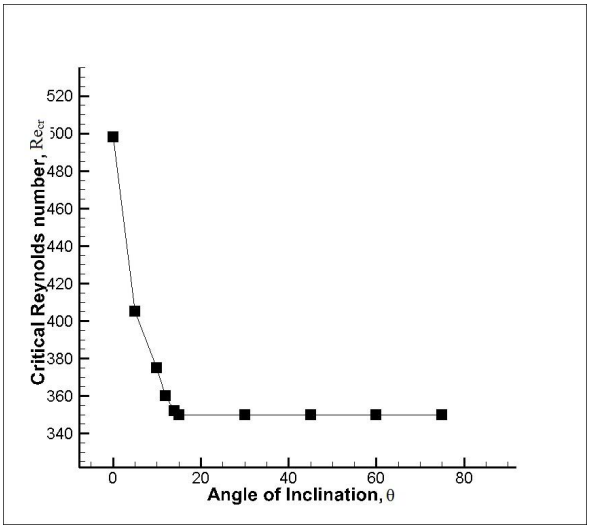

Figure 8: Critical Reynolds number Re_{cr} vs. Angle of Inclination, θ.

Figure 8 shows that the critical Reynolds number for angles between θ=0º and 15º is decreasing with

the increase of the angle of inclination. The critical Reynolds number for backward facing step for θ=0º was reported to be around 500 (Armaly et.al. 2003) (Chen et.al. 2006) and was found in the present study to be at Re=498. For θ=5º the flow critical Reynolds umber was found to be at Re=405. This trend of decreasing critical Reynolds number with the increase in the angle of inclination from θ=0º and 15º, could be attributed to the length of the neck of the vortex in the wake of the inclined step. As the angle of inclination increases the length of the vortex neck increases, therefore the rolling up shear layer can separate the vortex from the neck and dissipate more easily into the wake of the inclined step than in the case of the backward step. The various critical Reynolds numbers obtained for different angles of inclination were fitted into a polynomial to derive a generic equation representing the variation of critical Reynolds number with the increase of inclination angle, presented in equation (17).

$$\mathrm{Re_{cr}} = (-0.0000018)\theta^5 + (0.000395)\theta^4 - (0.032748)\theta^3 + (1.264546)\theta^2 - (22.514803)\theta + 496.159 \quad (17)$$

It is also important to realize that the steady state vortex presented in figure 6 from Chen et al (2006), for an angle of inclination, θ=45º and for a Reynolds number of Re=343, is identical to the vortex presented in figure 7(c) in the present paper. The analysis done in Chen et.al. (2006) was in 3-Dimensions and in a constrained flow setup, to simulate the flow in a duct with an inclined edge. The characteristics of the flow are expected to be similar to that of the steady state vortex presented herein, as the vortex at the center of the domain in a duct is most comparable to the 2D vortex in the wake of the unconfined flow past an inclined step.

4.4 Unsteady and periodic flow analysis:

As presented in the previous section, the critical Reynolds number for inclination angles between 15º and 75º was found to be 350, therefore in order to visualize unsteady periodic vortex shedding, in the present section simulations were undertaken for Reynolds numbers of 500 and 800. Under these conditions flow remains laminar, since as determined by Armaly et al (1983) the flow over an inclined step is laminar whenever Reynolds number is below 1200.

The onset of vortex shedding in the case of the backward facing step or inclined step occurs due to the rolling up shear layer, located downstream of the inclined step. The rolling up shear layer is generated due to the interaction between the negative momentum of the vortex in the wake of the step and the solid constrained boundary located below the vortex. This mechanism is different from the one appearing in a generic bluff body, where vortex shedding occurs due to the flapping motion of the upper and lower vortices appearing at the body trailing edge, vortices shed alternately into the wake.

Laminar periodic vortex shedding is described in the present section in Figures 9 to 14, with the help of instantaneous streamlines and vorticity contours corresponding to six equally spaced time instants within a shedding cycle of time period T. Reynolds number was taken to be 500 in figures 9 to 13 and 800 in figure 14. Each figure presents the results for a given inclination angle. Inclination angles vary between 15º in figure 8 to 75º in figure 12, the inclination angle of figure 13 is 15º. Notice that in all figures, the vortex forms at the inclined edge vertices of the inclined step and is shed into the wake. Two types of inviscid critical points, namely ‘centre’ and ‘saddle’ can be seen from the figures. A critical point is a location where slope of streamline becomes indefinite; the point of zero velocity is referred to as the ‘centre’ while the point where two streamlines running in opposite direction touch each other is referred to as the ‘saddle’. From the present study, it is realized that whenever Re >350, the saddle point of a shed vortex, disappears before a new vortex is shed. Instantaneous vorticity contours, shown in Figure 9 to14, further reveals the formation and shedding of vortices from the

inclined edge vertex of the step. Due to its streamlined shape, separation in an inclined step always occurs at the inclined edge vertex leading to a separated shear layer from the vertex which is stretched, bent and finally convected into the wake. The neck between the tip and the main body of a growing vortex stretches and bends, leading to separation from the main body.

The positive and negative vorticity, corresponding to counter-clockwise and clockwise motion, is shown by solid and dashed lines, respectively. The rolling up shear layer exhibits a flapping motion while the shear layer moves into the growing vortex in the wake only to be convected downstream in the form of vortical structure which scales with the height of the inclined step. It is interesting to point out that, the same mechanism and features of vortex shedding has been found for all different angles studied. The evolution of the recirculating vortex in the wake of the step before being shed can be clearly seen in the figures 9-14

The results at Re=800, shown in Figure 14, reveals the same shedding mechanism as the one found at lower Reynolds. Based on quantitative observations made from the simulations, it was evident that at Reynolds number 500, the vortex dissipation is more organized, but the simulations at Reynolds 800, showed much faster and disorganized vortex dissipation. This is due to the fact that as Reynolds number increases, the kinetic energy associated to each fluid particle also increases and momentum interchange between particles increases, producing a quicker and higher disorganized vortex dissipation. Vortex shedding frequency for all the cases studied, which is presented in the next section, was found to be very similar regardless of the Reynolds number and inclination angle. This fact emphasizes the global nature of flow dynamics. A detailed three-dimensional calculation is needed to explore the three-dimensional nature of the flow at moderate Re and to determine the exact Reynolds number for the flow transition from two-dimensions to three-dimensions.

The vortex recirculation length, under unsteady state conditions, varies with time from the formation of the vortex until it is finally dissipated into the wake after its separation. From figure 9(i) the vortex recirculation length, when the vortex is just formed, was 2 units, and it increased to 4 units when it was finally separated by the rolling up shear layer, as presented in figure 9(g), (h). Similar movement of recirculating vortex can also be observed in figures 10 to 14 within a vortex shedding cycle.

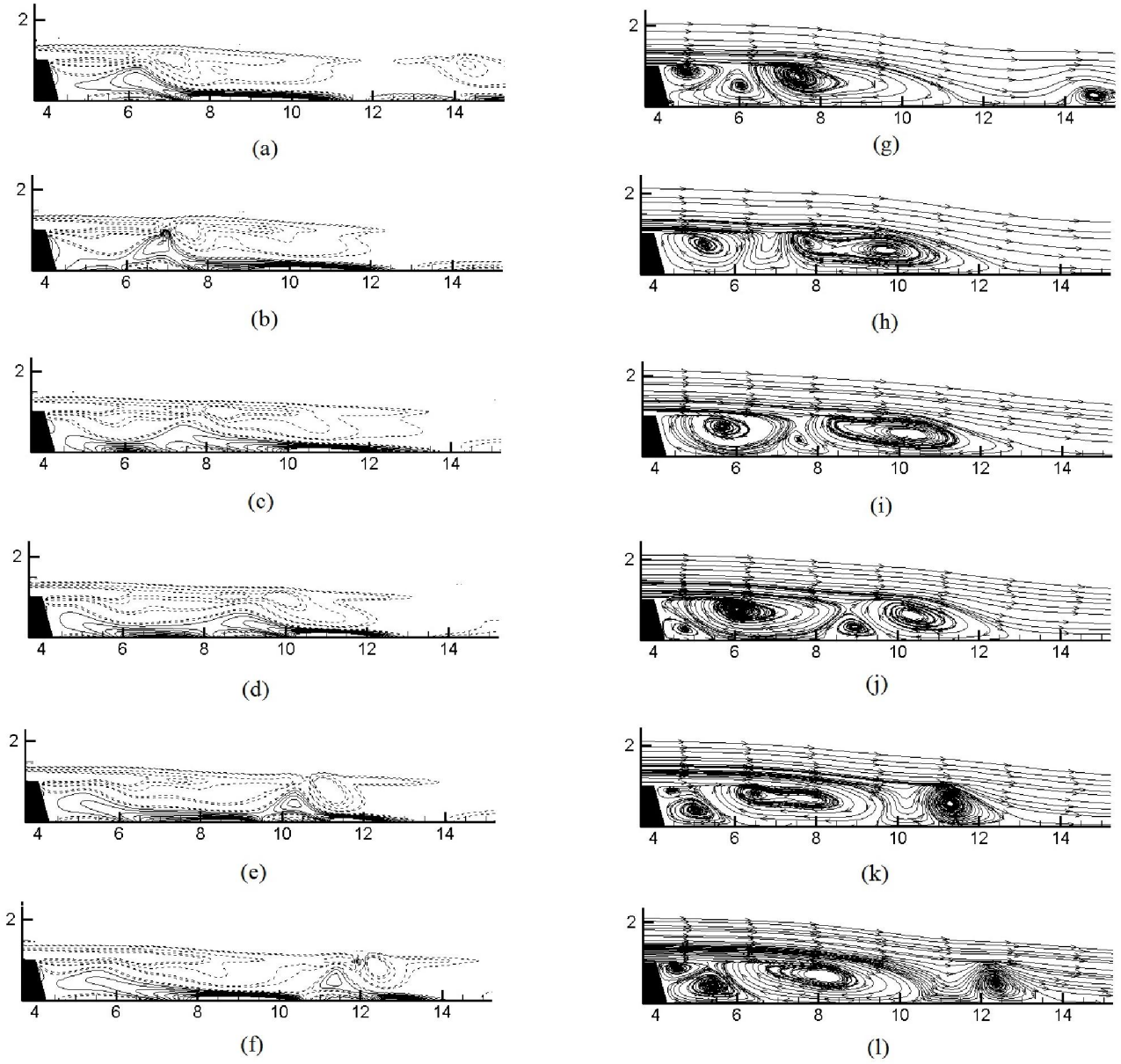

Figure 9: Vorticity and corresponding Streamline plots of vortex shedding cycle in the wake of Inclined Step with inclination angle θ=15º, for Re 500, upstream length ul=4a, and six time steps: (a, g) T/6; (b, h) T/3; (c, i) T/2; (d, j) 2T/3; (e, k) 5T/6; (f, l) T.

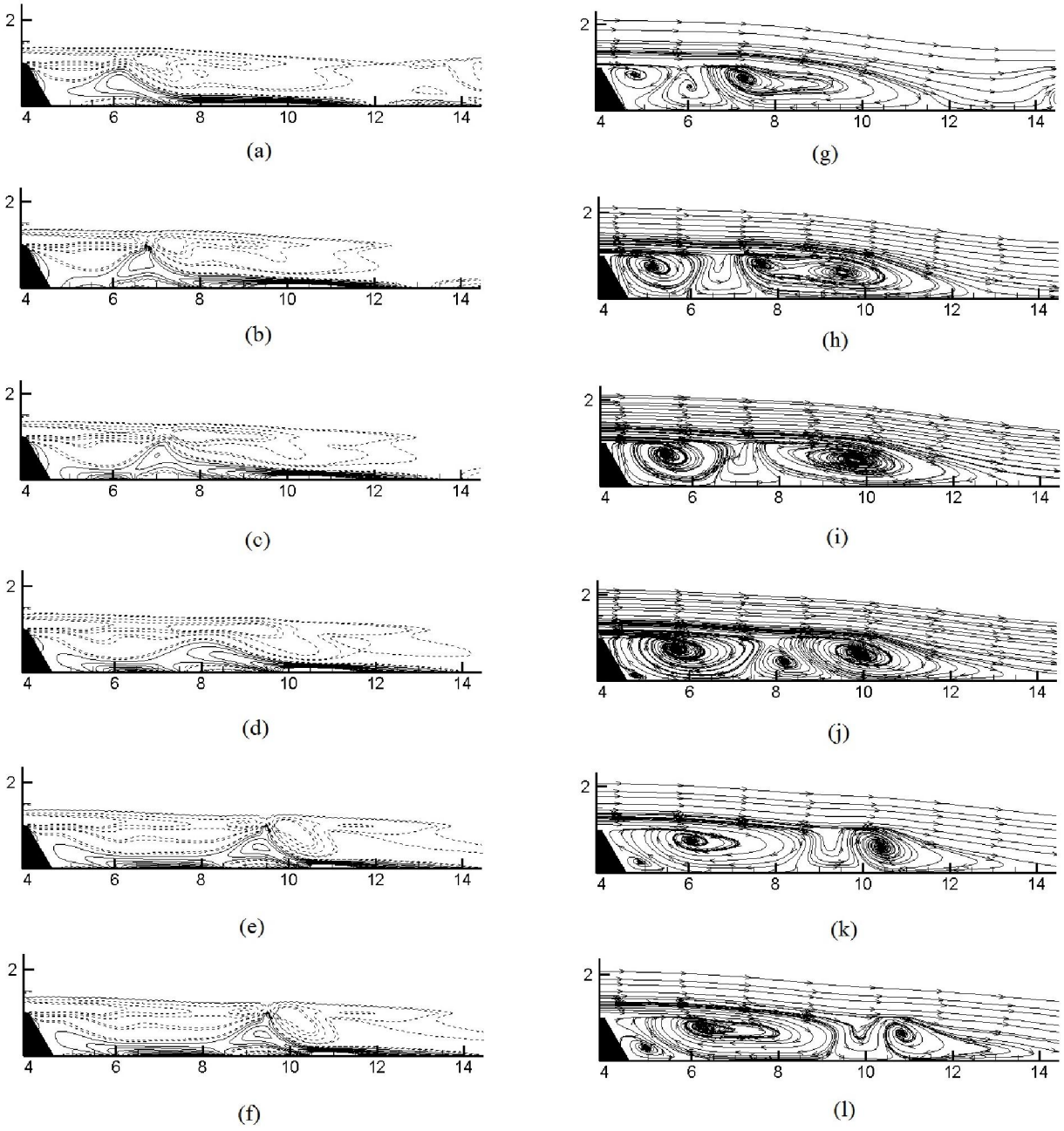

Figure 10: Vorticity and corresponding Streamline plots of vortex shedding cycle in the wake of Inclined Step with inclination angle θ=30º, for Re 500, upstream length ul=4a, and six time steps: (a, g) T/6; (b, h) T/3; (c, i) T/2; (d, j) 2T/3; (e, k) 5T/6; (f, l) T.

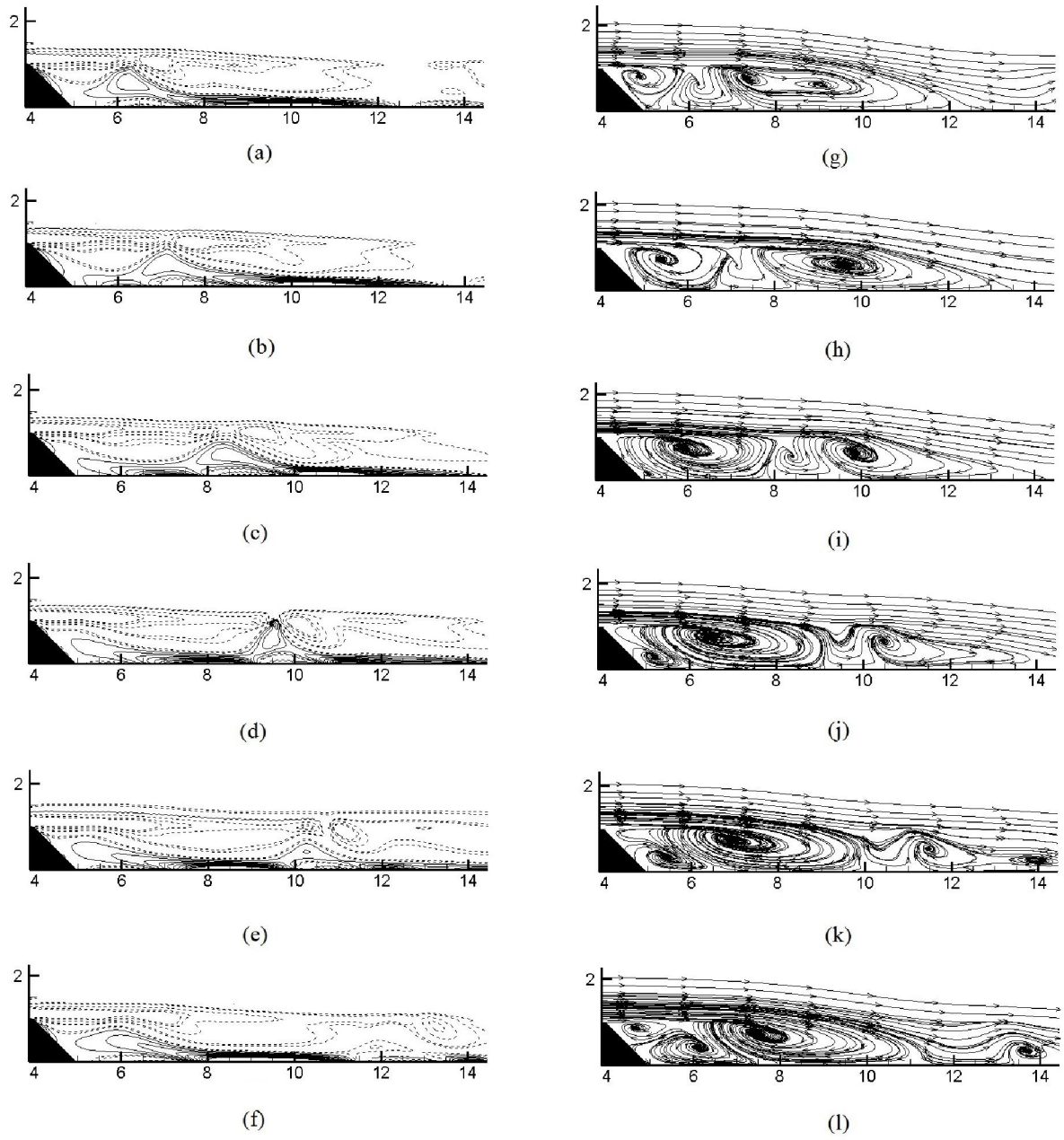

Figure 11: Vorticity and corresponding Streamline plots of vortex shedding cycle in the wake of Inclined Step with inclination angle θ=45º, for Re 500, upstream length ul=4a, and six time steps: (a, g) T/6; (b, h) T/3; (c, i) T/2; (d, j) 2T/3; (e, k) 5T/6; (f, l) T.

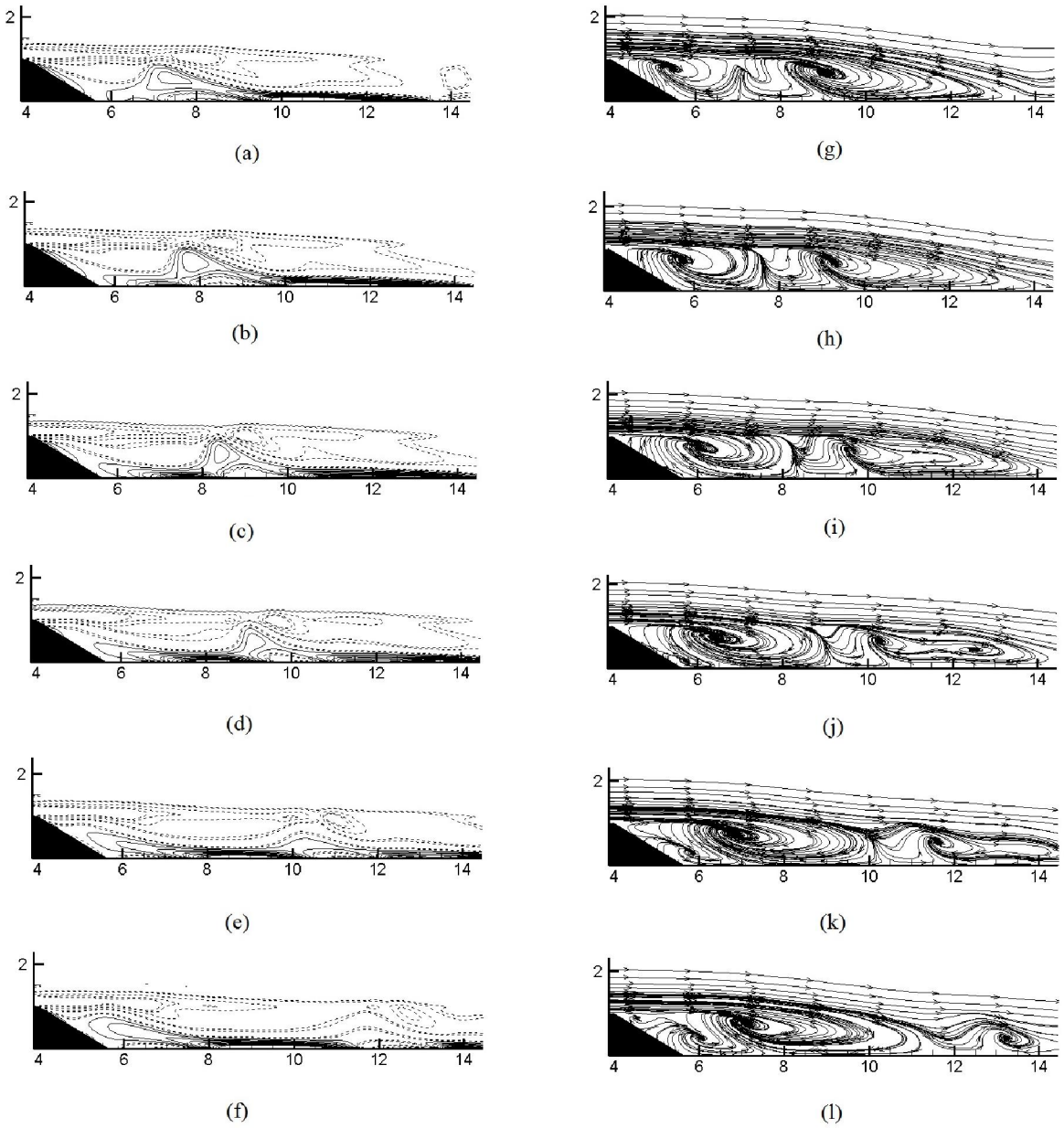

Figure 12: Vorticity and corresponding Streamline plots of vortex shedding cycle in the wake of Inclined Step with inclination angle θ=60º, for Re 500, upstream length ul=4a, and six time steps: (a, g) T/6; (b, h) T/3; (c, i) T/2; (d, j) 2T/3; (e, k) 5T/6; (f, l) T.

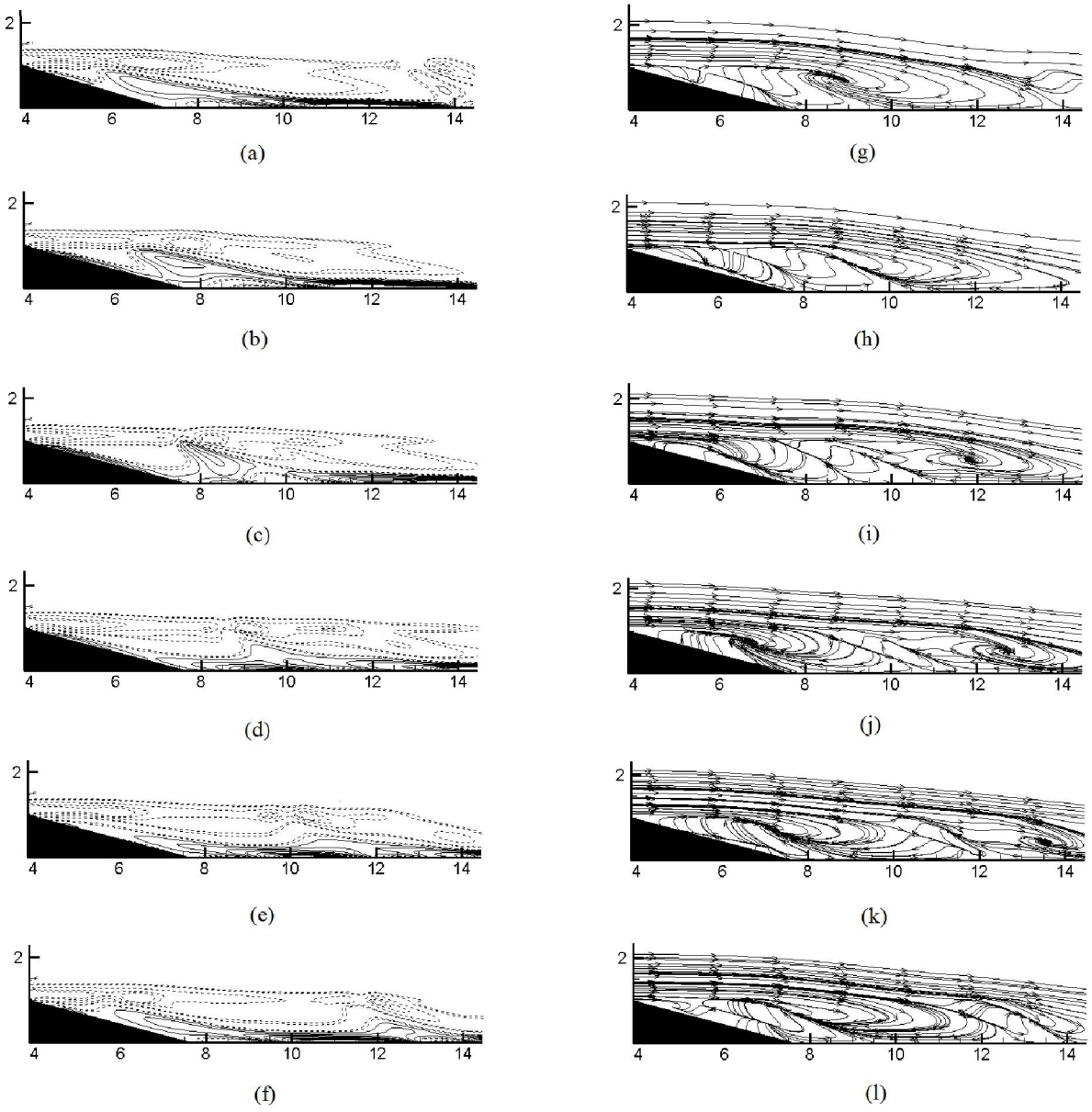

Figure 13: Vorticity and corresponding Streamline plots of vortex shedding cycle in the wake of Inclined Step with inclination angle θ=75º, for Re 500, upstream length ul=4a, and six time steps: (a, g) T/6; (b, h) T/3; (c, i) T/2; (d, j) 2T/3; (e, k) 5T/6; (f, l) T.

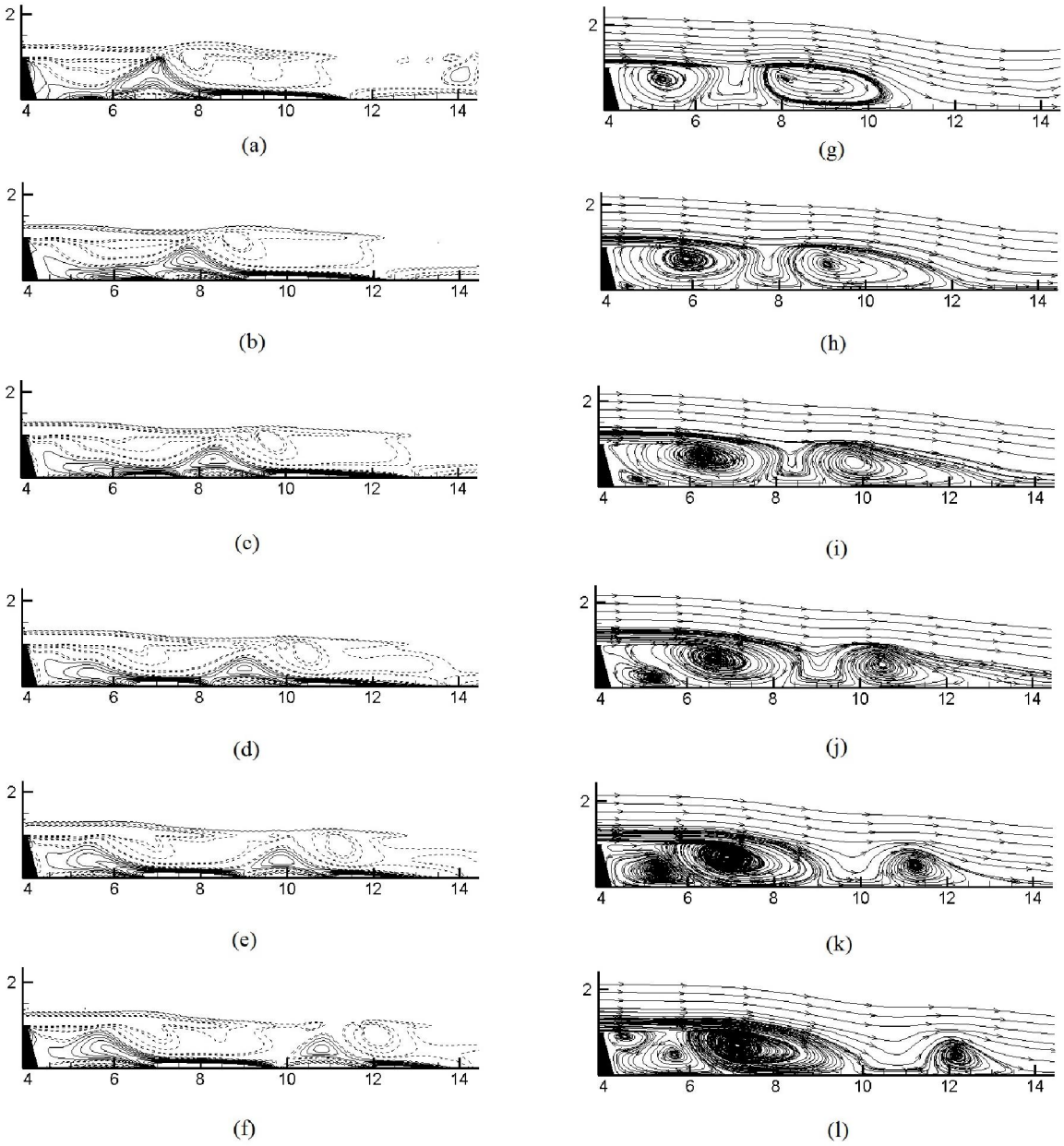

Figure 14: Vorticity and corresponding Streamline plots of vortex shedding cycle in the wake of Inclined Step with inclination angle θ=15º, for Re 800, upstream length ul=4a, and six time steps: (a, g) T/6; (b, h) T/3; (c, i) T/2; (d, j) 2T/3; (e, k) 5T/6; (f, l) T.

4.5 Lift and drag coefficients.

Figures 15 and 16, present the variation of averaged lift and drag coefficients acting on the inclined step with the change of inclination angle. These coefficients consider the average normal and shear stresses acting on the upstream horizontal surface and the inclined step surface. To calculate lift and drag coefficients, the expressions presented in equation (18) were used. It is important to realize that as the flow under study is unsteady and periodic, the concept of average lift and drag coefficients has to be used.

$$C_D = \frac{F_D}{\frac{1}{2}\rho U^2 a^2}, \qquad C_L = \frac{F_L}{\frac{1}{2}\rho U^2 a^2} \tag{18}$$

F_D and F_L are respectively the dimensional drag and lift forces consisting of their respective components of normal, F_p and shear, F_s forces acting on the upstream horizontal and inclined surfaces. The pressure and shear forces acting on the inclined step are calculated by the expressions presented in equation (19).

$$F_p = -(p.A)\,\hat{n}, \qquad F_s = -\mu A\left(\frac{\partial u_i}{\partial x_j}\right).\hat{n} \tag{19}$$

Where $\hat{n}$ is the unit normal vector perpendicular to the surface. Drag force was taken as positive when pointing towards the positive X axis direction, and Lift force was regarded as positive when pointing towards the positive Y axis direction.

From figures 15 and 16, it can be observed that regardless of the Reynolds number and the upstream horizontal length used, the averaged drag coefficient, C_D is inversely proportional to the angle of inclination increase, averaged lift coefficient, C_L is directly proportional to the angle of inclination. This trend is due to the fact that as the inclination angle increases, the inclined surface area also increases, therefore, the component of the vertical force on the Y direction due to the pressure acting on the inclined surface will also increase; see figure 16 (a) and (b). It can also be observed that, regardless of the inclination angle, lift coefficient for an upstream horizontal length of ul=4a, it is always higher than for smaller lengths, since, as the horizontal upstream length increases, the area where the normal pressure is acting also increases. Lift coefficient increase, is smaller when the upstream horizontal length goes from a to 2a than from 2a to 4a, this happens regardless of the angle of inclination and Reynolds number. This small increase is due to the increase in the area of the horizontal upstream surface on which the normal pressure is acting. When comparing figures 16(a) and (b), it is realized that, regardless of the inclination angle, as Reynolds number increases the lift coefficient suffers a small increase. This can be attributed to the pressure distribution on the surface of the inclined step, as Reynolds number increases the relative pressure acting on the upstream surface suffers a small decrease, the pressure decrease over the inclined surface, is even smaller, as can be seen in figures 17 (a) and (d).

Regarding the averaged drag coefficient, figure 15 shows that drag coefficient decreases with the inclination angle increase. This can be attributed to the fact that as the angle of inclination increases, shear stresses acting on the inclined surface increase, due to the area increase. As a result of the downstream vortices generated, the increase of shear stresses appearing onto the inclined surface, has the opposite direction than the ones appearing onto the upper surface. Therefore, the overall shear

stresses component acting in the X direction will decrease with the inclination angle increase. On the other hand, the drag component due to the normal pressure acting over the inclined step generates a force rather constant and independent of the inclined step angle, this force will pull the step towards the positive direction, because the relative pressure onto the inclined surface is negative. Figures 17 (a) and (d), shows that, pressure onto the inclined surface, suffers a marginal increase as the inclined step angle increases. Since pressure forces are positive and the inclined step shear forces increase in the opposite direction with the increase of inclined step angle, the drag on the body will decrease as the inclination angle increases.

For a given angle of inclination, as the upstream horizontal length increases the shear stresses onto the horizontal surface also increase, but the pressure acting on the inclined surface vary marginally as seen in figure 17 (c) and (f), causing the drag coefficient to increase.

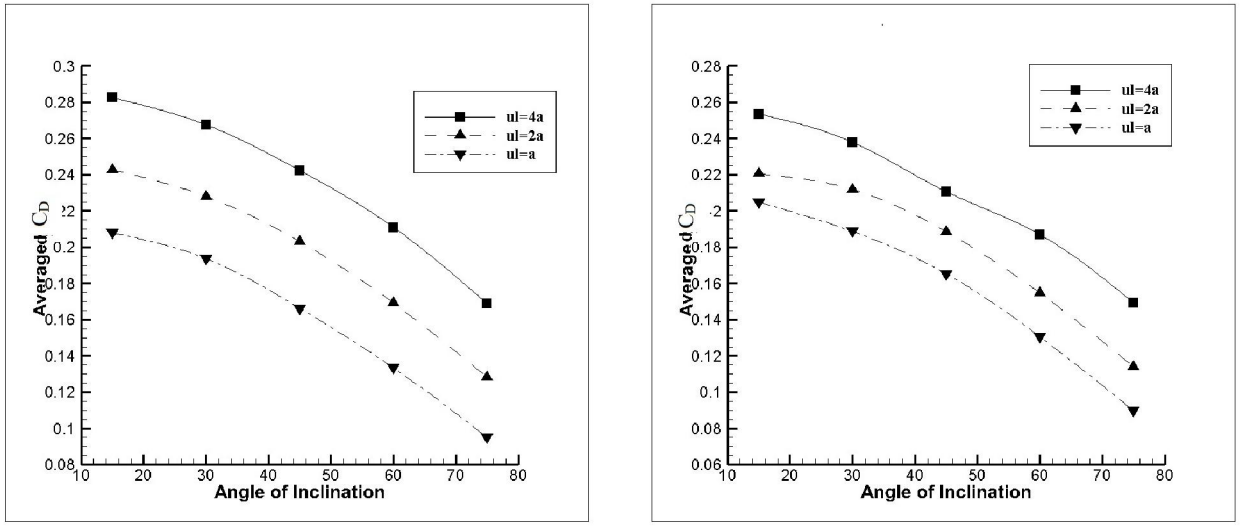

Figure 15: Averaged Drag coefficient versus angle of Inclination: (a) Re=500 (b) Re=800

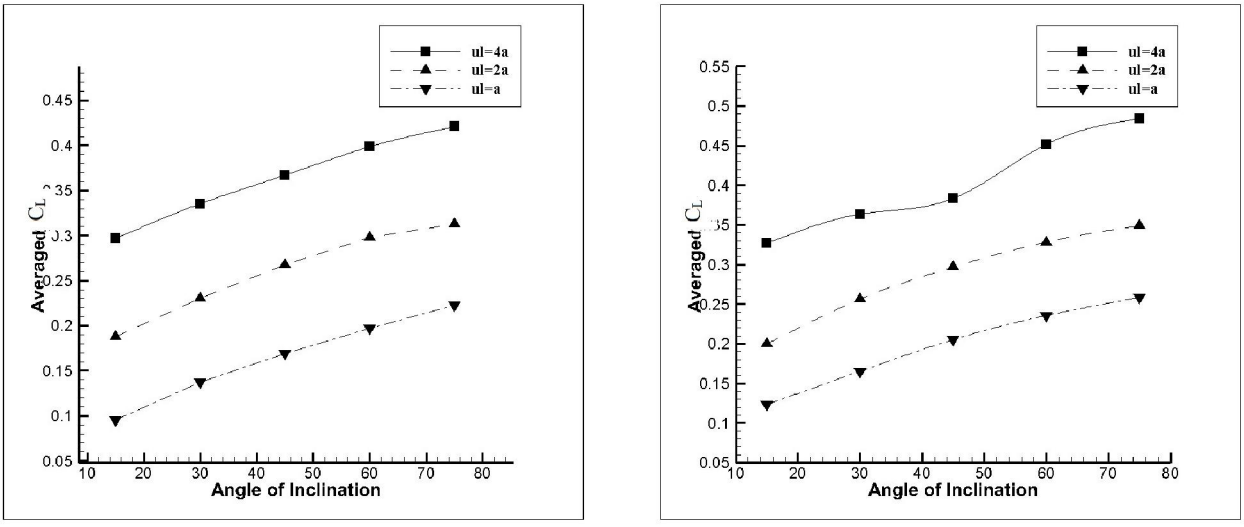

Figure 16: Averaged Lift coefficient versus angle of Inclination. (a) Re=500 (b) Re=800

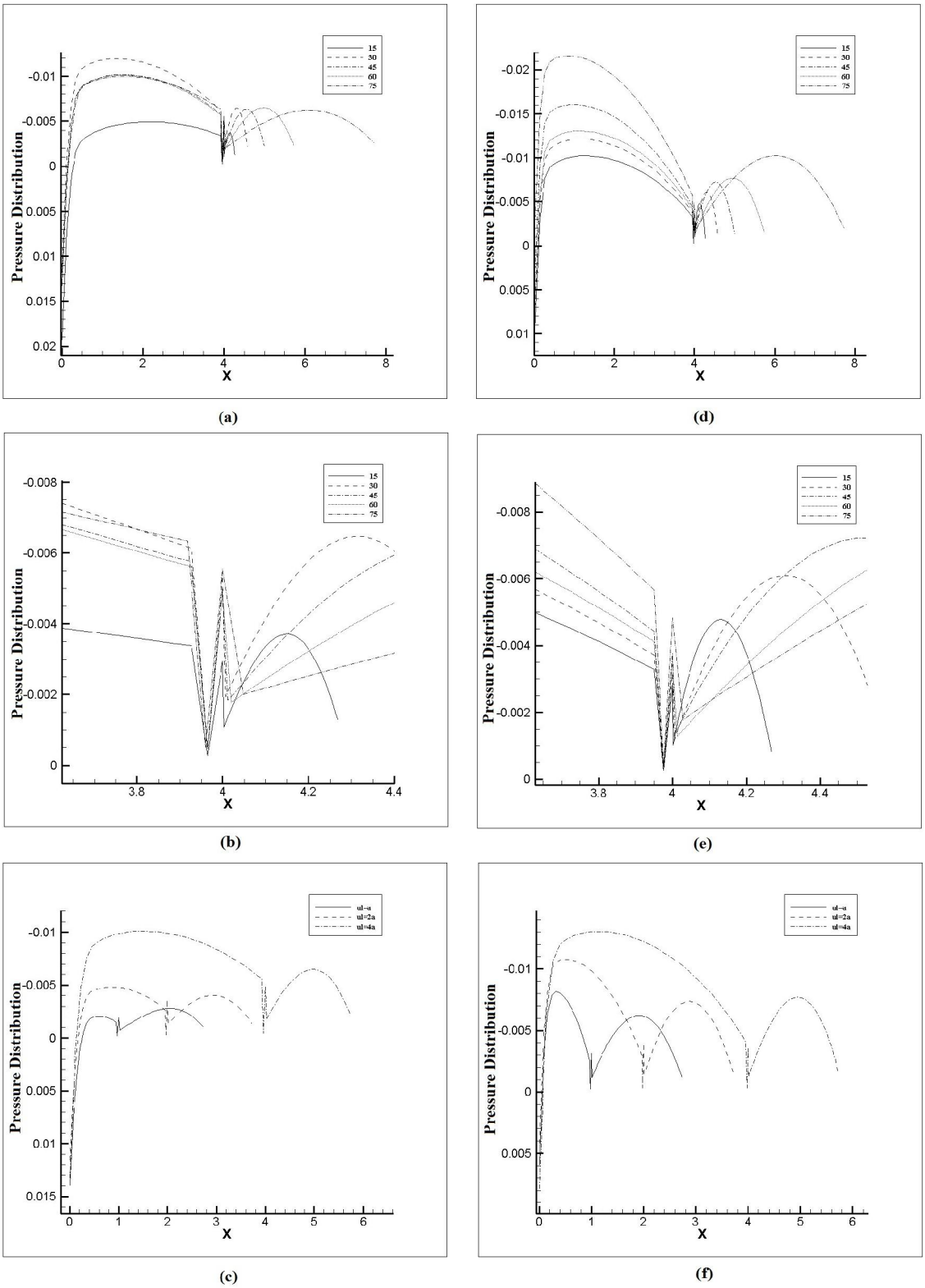

Figure 17: Instantaneous Pressure Distribution plots on the inclined step surface. (a) For different angles of inclination, θ at Re=500. (b) Close up view of the step corner at Re=500. (c) For different upstream length, ul at Re=500 and θ=60^o . (d) For different angles of inclination, θ at Re=800. (e) Close up view of the step corner at Re=800. (f) For different upstream length, ul at Re=800 and θ=60^o.

Figure 17 presents the instantaneous non dimensional pressure distribution plots on the complete inclined step surface. Relative pressure acting on the step surface is negative since the velocity of fluid is higher on the surface of the step than the free stream velocity as in the case of the top surface of an airfoil. In figures 17 (a) and (d), the pressure distribution on the step surface is presented for all the inclination angles simulated at Re=500 and 800 respectively. It can be observed that as the as the angle of inclination increases, the pressure acting on the upstream surface decreases, causing the lift on the body to increase, as seen in figure 16(a) and (b). The variation of pressure on the inclined surface suffers a marginal increase with the increase in the Reynolds number, as can be seen in figures 17 (a) and (d); (c) and (f). An interesting observation that can be made on the right corner of the upstream surface, where the inclined surface of the step starts, is the pressure fluctuation. The close up view of these pressure fluctuations can be seen clearly in figure 17 (b) and (e). These pressure fluctuations could be due to the sudden change in geometry at the corner, leading to variations in the velocity of the flow. An important phenomenon to be observed from figures 17 (a) and (d) is that the pressure, on both, the upstream and inclined surfaces, first decreases until reaching the midpoint of their respective surfaces and then increase. This behavior is due the velocity profile development on the respective surfaces. When the upstream surface is increased for a given angle of inclination, the pressure on the upstream surface tends to decrease, being this decrease directly proportional to the upstream length, as presented in figure 17 (c) and (f). But the increase in the upstream surface length, have a minimal effect on the pressure distribution over the inclined surface, the pressure tends to marginally decrease. The decrease in pressure when the Reynolds number is increased for a given angle and upstream surface is also very marginal in both cases, as presented in figures 17 (a) and (d) and figures 17 (c) and (f).

Figure 18, presents the time dependent drag profile for different angles of inclination, 15º, 45º, 75º and at different Reynolds numbers 500 and 800. It can be observed that for a given Reynolds number, the frequency of oscillation has a negligible change with the increase of inclination angle, see figures 18 (b) and (d). It can also be observed that if the inclination angle is maintained constant and Reynolds number is increased, the oscillation frequency increases about 30% when the Reynolds number goes from 500 to 800. This pattern shows the global nature of the flow.

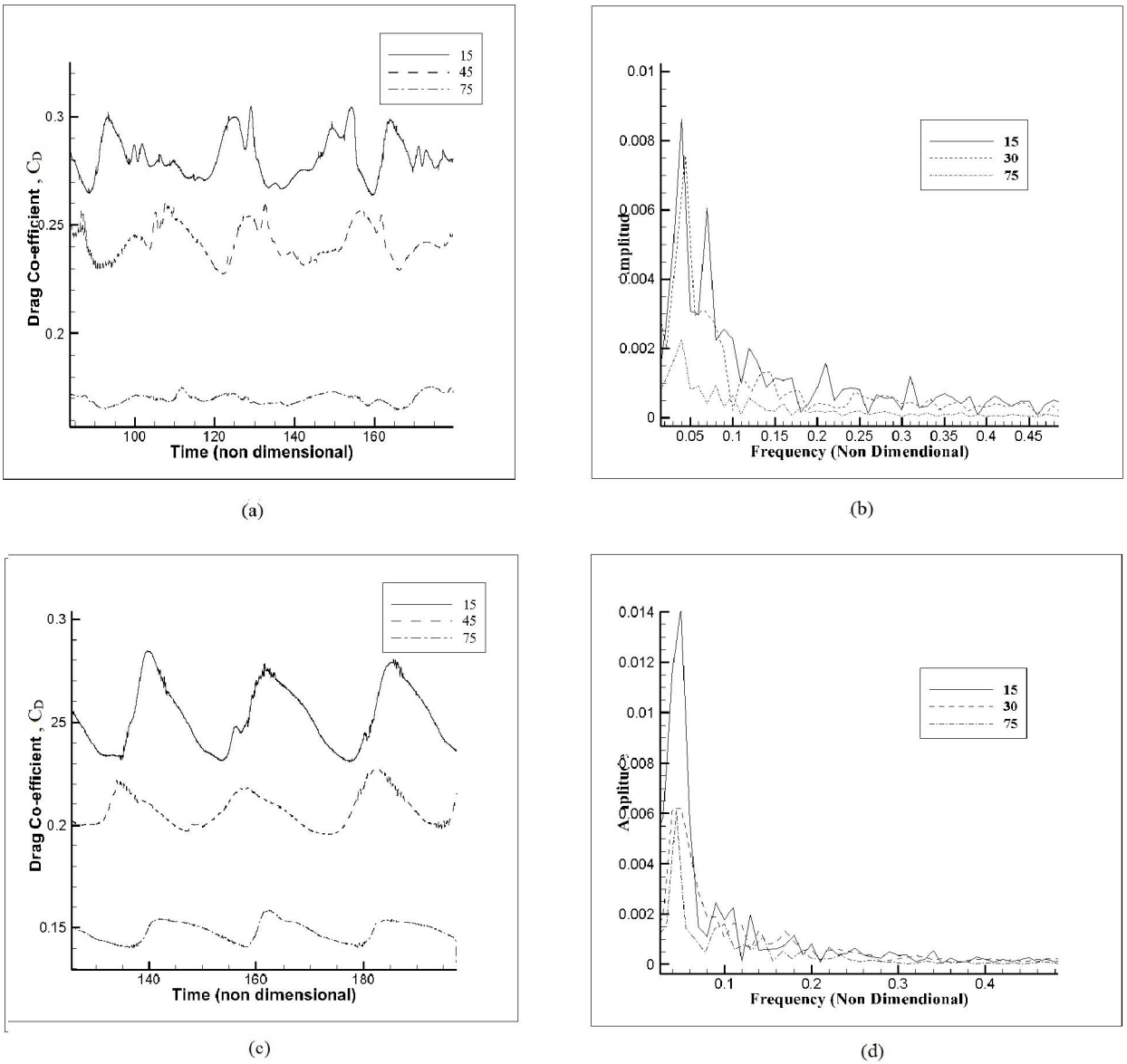

Figure 18: Drag coefficient versus time for L=4a. (a) Re=500. (b) FFT analysis of C_D at Re=500. (c) Re=800. (d) FFT analysis of C_D at Re=800

The drag coefficient amplitude of oscillation decreases with the increase of inclination angle, the decrease being of over 75% when the inclination angle goes from 15º to 75º for Re=500, see figures 18 (b) and (d). The amplitude decrease with the inclination angle increase is smaller as the Reynolds number increases.

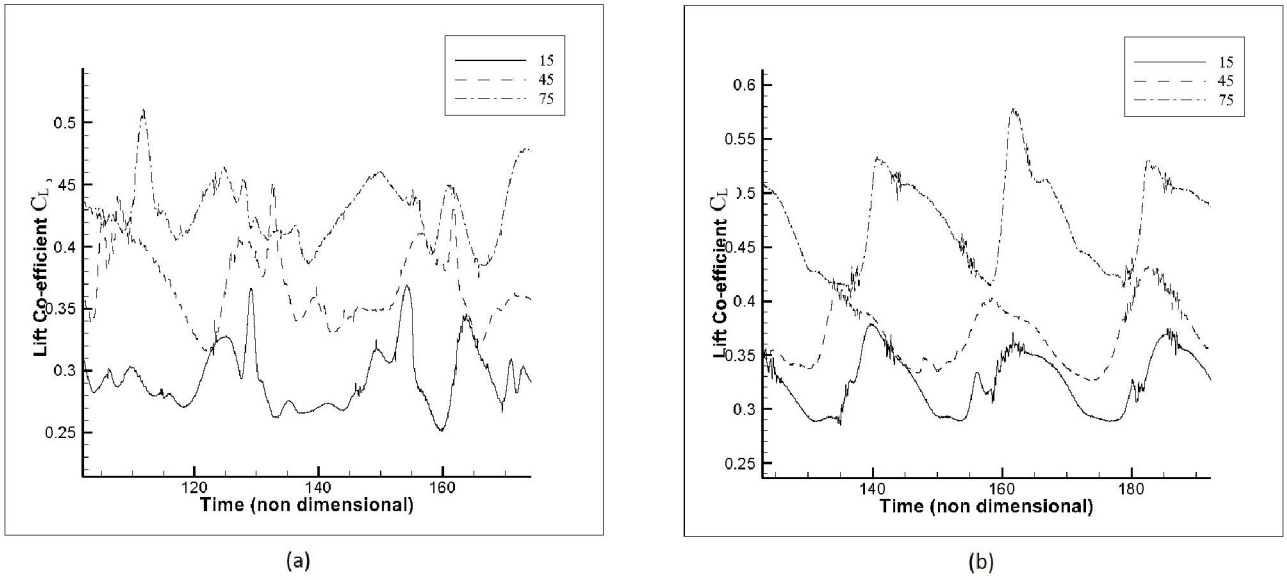

Figure 19: Lift Coefficient versus time for L=4a (a) Re=500 (b) Re=800

Figure 19, presents the time dependent lift coefficient profile for the same different angles of inclination and Reynolds numbers introduced in figure 18. It is interesting to note that the oscillation amplitude variation with the inclination angle or Reynolds number increase is much smaller than in the case of drag coefficient. In other words, the amplitude has an increase of 50% when inclination angle goes from 15º to 75º, but this happens at Reynolds number 800, for Reynolds number = 500, no appreciable variation was observed.

5. Conclusions:

1. In the steady state analysis, it has been found that the vortex recirculation length has a strong dependency of Reynolds number. Recirculation length remains constant for all angles of inclination studied.
2. The effect of the boundary layer onto the upstream horizontal surface has a negligible effect on the vortex recirculation length, and on the downstream periodic flow.
3. Vortex shedding was found to be occurring at Reynolds number of 350 and inclination angles between 15º and 75º. For angles of inclination below 15º the critical Reynolds number for flow transition from steady state to periodic unsteady (vortex shedding), increases with the decrease of inclination angle.
4. The average drag coefficient on the body decreases as the angle of inclination increases. This is attributed to the inclined surface shear drag increase, in the opposite direction of the pressure and upstream surface shear drag.
5. Average lift coefficient increases with the angle of inclination increase. This is because the force component due to the pressure acting on the inclined surface increases with the inclination angle, due to the increase of the inclined surface area.
6. The average lift and drag acting on the inclined step increases with the increase in the upstream horizontal surface length for a given Reynolds number and angle of inclination.
7. From the quantitative observations in the vorticity plots, for the cases studied, flow appears to be more unsteady and disorganized with the Reynolds number increase.

8. Amplitude of oscillation tends to decrease as angle of inclination increases, the vortex shedding frequency increases by 30% as Reynolds number increases from 500 to 800.

References:

Anderson J.D. (1995) Computational Fluid Dynamics. McGraw Hill.

Armaly, B. F., Durst, F., Peireira, J. C. F., Schonung, B. (1983). Experimental and theoretical investigation of backward-facing step flow. J. Fluid Mech. 127: 473– 96.

Armaly, B. F., Li A, Nie JH. (2003). Measurements in the three-dimensional laminar separated flow. Int. J. Heat and Mass Transfer. 46: 3573-3582.

Chen Y.T., Nie J.H., Hsieh H.T., Sun L.J. (2006), Three-dimensional convection flow adjacent to inclined backward-facing step. Int. Journal of Heat and Mass Transfer. 49: 4795-4803.

Chowdhary H., Dhiman A., (2011). Two-Dimensional Laminar Fluid Flow and Heat Transfer over a Backward-Facing Step: Effects of Reynolds and Prandtl Numbers. Heat transfer research journal. 42, 4, 379-402

Cogotti A. (1998). A parametric study on the ground effect of a simplified car model. SAE paper 980031; 37-63.

Franck G; Nigro N; Storti M; D'elía J. (2009). Numerical simulation of the flow around the Ahmed vehicle model. Latin American Applied Research. 39: 295-306.

Gandjalikhan Nassab SA; Moosavi R; Hosseini Sarvari SM. (2009). Turbulent forced convection flow adjacent to inclined forward step in a duct. International Journal of thermal sciences. 48: 1319-1326.

Gartling, D. K. (1990). A test problem for outflow boundary condition flow over a backward-facing step. Int. J. Numer. Methods Fluids 11: 953–967.

Guilmineau E. (2008). Computational study of flow around a simplified car body. Journal of wind engineering. 96: 1207-1217.

Kaiktsis L; Karniadakis G. E; Orszag, S. A. (1991). Onset of three-dimensionality, equilibria, and early transition in flow over a backward-facing step. J. Fluid Mech. 231: 501–528.

Kaiktsis L; Karniadakis, G. E; Orszag, S. A. (1996). Unsteadiness and convective instabilities in a two-dimensional flow over a backward-facing step. J. Fluid Mech. 321: 157–187.

Kaltenbach, HJ; Janke, G.. (2000). Direct numerical simulation of flow separation behind a swept rearward-facing step at $Re_H = 3000$. Physics of Fluids, 129: 2320–2337.

Kaltenbach HJ. (2004). Turbulent flow over a swept backward-facing step. European Journal of Mechanics B/Fluids. 23; 501-518.

Kapadia S; Roy S; Wurtzler K. (2003). Detached eddy simulation over a reference Ahmed car model. AIAA paper 0857: 1-10.

Kim, J; Moin, P. (1985), Application of a fractional-step method to incompressible Navier-Stokes equations, J. Comput. Phys., 59: 308–323.

Kotapati R.B; Shock R; Chen H. (2014). Lattice-Boltzmann Simulations of Flows over Backward-Facing inclined steps. International Journal of Modern Physics C. 25; 1: 1340021-1-14.

Krajnovic S; Davidson L. (2004). Large-eddy simulation of the flow around simplified car model. SAE World congress, Detroit USA. Paper 01-0227: 1-10

Leinhart H; Stoots C; Becker S. (2003). Flow and turbulence structures in the wake of a simplified car model (Ahmed model). SAE Technical paper series. Paper 01-1315. 1-8.

Louda P; Príhoda J; Kozel K; Svácek P. (2013). Numerical simulation of flows over 2D and 3D backward-facing inclined steps. International Journal of Heat and fluid Flow. 43: 268-276.

Makiola B. (1992). Experimentelle Untersuchungen zur strömung über Schräge stufe. PhD Thesis Univ. of Karlsruhe.

Nguyen TD; Wells JC; Nguyen CV. (2012). Velocity measurement of near-wall flow over inclined and curved boundaries by extended interfacial particle image velocimetry. Flow measurement and instrumentation. 23: 33-39.

Roberts GO.(1971). Computational meshes for boundary layer problems. Proceedings of the Second International Conference on Numerical Methods and Fluid Dynamics, Lecture Notes in Physics. Springer-Verlag: New York. 8:171–177.

Sohankar, A., Davidson, L., Norberg, C., “Numerical simulation of unsteady flow around a square two dimensional cylinder,” 12th Australian Fluid Mechanics Conference, University of Sydney,Australia, 517-520, (1995).

Sohankar, A., Norberg, C., Davidson, L., "Low Reynolds number flow around a square cylinder at incidence: Study of blockage, onset of vortex shedding and outlet boundary condition,” Int Journal for Numerical Methods in Fluids,26, 39-56, (1998).

Williams, P. T., and Baker, A. J. (1997), Numerical simulations of laminar flow over a 3D backward-facing step. Int. J. Numer. Methods Fluids 24: 1159–1183.